



CO₂ Electroreduction to Multicarbon Products from Carbonate Capture Liquid

Geonhui Lee^{1†}, Armin Sedighian Rasouli^{1†}, Byoung-Hoon Lee^{1†}, Jinqiang Zhang¹, Da Hye Won², Yurou Celine Xiao³, Jonathan P. Edwards³, Mi Gyoung Lee¹, Eui Dae Jung¹, Fatemeh Arabyarmohammadi³, Hengzhou Liu^{4,5}, Ivan Grigioni¹, Jehad Abed¹, Tartela Alkayyali³, Shijie Liu³, Ke Xie¹, Rui Kai Miao³, Sungjin Park¹, Roham Dorakhan¹, Yong Zhao³, Colin P. O'Brien³, Zhu Chen¹, David Sinton³, Edward Sargent^{1,4,5*}

¹Department of Electrical and Computer Engineering, University of Toronto, 35 St George Street, Toronto, Ontario, M5S 1A4, Canada

²Clean Energy Research Center, Korea Institute of Science and Technology (KIST), Seoul 02792, Republic of Korea

³Department of Mechanical and Industrial Engineering, University of Toronto, 5 King's College Road, Toronto, Ontario, M5S 3G8, Canada

⁴Department of Chemistry, Northwestern University, Evanston, Illinois 60208, United States



⁵Department of Electrical and Computer Engineering, Northwestern University, Evanston, Illinois 60208, United States

*Correspondence: ted.sargent@utoronto.ca / ted.sargent@northwestern.edu

†These authors contributed equally to this work

SUMMARY

Alkali hydroxide systems capture CO₂ as carbonate; however, generating a pure CO₂ stream requires significant energy input, typically from a thermal cycling to 900°C. What is more, the subsequent valorization of the gas-phase CO₂ to products introduces additional energy requirements and system complexity, including managing the formation of (bi)carbonate in an electrolyte and separating unreacted CO₂ at the downstream. Here we report the direct electrochemical conversion of CO₂, captured in the form of carbonate, into multicarbon (C₂₊) products. Using an interposer and a Cu/CoPc-CNTs electrocatalyst, we achieve 47% C₂₊ Faradaic efficiency at 300 mA cm⁻² and a full cell voltage of 4.1 V. We report 56 wt.% of C₂H₄ and no detectable C₁ gas in the product gas stream: CO, CH₄ and CO₂ combined total below 0.9 wt.% (0.1 vol.%). This approach obviates the need for energy to regenerate the CO₂ loss, an issue seen in prior CO₂-to-C₂₊ reports.

Reactive capture; direct air capture; carbon capture and utilization; high CO₂ utilization; *in situ* CO₂ generation; ethylene; ethanol; electrochemical regeneration of capture liquid; system architecture of electrolyzer; molecular catalyst

INTRODUCTION

CO₂ capture from air and oceans, when combined with an upgrade into chemicals that serve as precursors to long-lived materials, offers to contribute carbon-negative (cradle-to-gate) solutions to offset difficult-to-abate emissions on the path to net-zero emissions.¹⁻³ Reactive capture systems unite CO₂ capture with CO₂ upgrade/utilization into more valuable chemicals. Much progress has been made electrochemically generating CO from captured CO₂, on the path to fuels and chemicals via syngas processes;⁴⁻⁸ in thermochemistry, reactive capture has proceeded to methane, methanol, and formate.⁹⁻¹¹

C₂ and higher products (C₂₊) represent a large global market: ethylene and ethanol lie in the range of ~US\$230B and ~US\$160B respectively,^{12,13} in contrast with the C₁ chemicals (CO and formic acid) generated by reactive capture to date, whose combined values are below US\$12B.^{14,15} Yet, to date, it is mainly C₁ products that have been produced in reactive capture systems of both electrochemical and thermochemical types.

Direct air capture (DAC) using alkali hydroxide captures CO₂ as carbonate and generates a pure/concentrated gas-phase CO₂ stream via thermal swing at ~ 900°C.¹⁶ The subsequent valorization of gas-phase CO₂ into value-added products introduces further energy losses and system complexity. This approach involves introducing CO₂ in the gas phase for electrolysis.

In contradistinction, reactive capture takes the carbon source from carbonate species, bypassing CO₂ concentrating steps. In prior reports of reactive capture from carbonate, Li et al. demonstrated pure syngas production with Faradaic efficiency (FE) of ~ 30% CO and ~70% H₂, and with a Cu electrocatalyst, ~14% C₂ FE was observed.⁵ The authors reported no appreciable loss of CO₂ during carbonate electrolysis. Such prior studies offer a path to avoid the energy-intensive steps associated with concentrating CO₂ and regenerating lost CO₂; however, until now, the selectivity toward more valuable CO₂-derived products has been limited compared to the diversity of products available in electrochemical CO₂ reduction reaction (CO₂RR) systems.

Such electrochemical CO₂RR systems, while they have achieved impressive increases in performance,^{17,18} suffer – in the case of alkaline and neutral CO₂RR – from low CO₂ utilization (the fraction of input CO₂ converted into desired products) that is ≤ 25% in the case of C₂ production due to carbonate formation in locally alkaline conditions.¹⁹ The low CO₂ utilization leads to a high cost to regenerate (otherwise-lost/emitted) CO₂.^{19,20} Enticingly, recent studies have overcome this CO₂ utilization limit via local CO₂ regeneration;²¹⁻²³ however, until now, the product gas stream has still been diluted by

Cradle-to-gate carbon negative technologies, including direct air capture (DAC), have shown promise in mitigating CO₂ emissions. However, these emerging technologies to capture CO₂ from air rely on a thermal swing to release concentrated CO₂, and today this comes at a high energy cost. The ensuing step in gas-phase CO₂ electrolysis requires additional energy. Furthermore, this step suffers from incomplete CO₂ conversion. It leads to a high cost to regenerate/separate (otherwise-lost/unreacted) CO₂. To tackle these challenges, a scheme known as reactive capture has been proposed: the integrated systems for capture-and-upgrade of CO₂ to valuable products. This approach is the direct conversion of chemisorbed CO₂ into value-added products. The benefits of reactive capture are: 1) to avoid the energy-intensive and carbon-positive steps associated with concentrating CO₂, 2) to enable ~ 0% reactant losses. This obviates the need for energy to regenerate/separate lost/unreacted reactants.



unreacted CO₂ and gas-phase CO₂-derived products such as carbon monoxide and methane.^{22,24,25} Even in systems that achieved > 76% CO₂ utilization via local CO₂ regeneration, unreacted CO₂ remains > 56 wt.% (Table 1).

Since CO₂ separation is an energy-intensive process (2-4.4 GJ/tonne of CO₂),^{16,26,27} unreacted CO₂ significantly increases overall system energy requirements. Eliminating CO₂ at the downstream could lead to a lower cost of purification demand.^{20,28}

Here we pursue C₂₊ products from carbonate solution – a liquid used in direct air capture – in an electrochemical reactive capture system. Among the striking results is a negligible presence (sub 1%) of CO₂ and C₁ gas products such as CO and CH₄ in the electrolyzer outlet, a finding promising for the minimization of product separation costs.

RESULTS

Modeling of carbonate electrolysis.

In prior reports of reactive capture from carbonate,⁵ *in situ* CO₂ is regenerated via an acid/base reaction between carbonate and protons. Protons come from the cation-exchange layer (CEL) of a bipolar membrane (BPM) under reverse bias. The *in situ* CO₂ is converted to CO₂-derived products at the surface of a Cu electrocatalyst, with C₂ (e.g., to ethylene and ethanol) selectivity totaling below 14% (Fig. S1).

We used modeling of chemical species generation, consumption, and diffusion to seek an explanation of why C₂₊ productivity is low in prior reactive capture studies, and to identify system architectures to increase it (Fig. 1b, Supplementary Note 1 and Supplementary Note 2). The modeling results show that the spacing between the CEL of BPM and the electrocatalyst influences species concentrations in the reactive capture system (Fig. S2-6). The concentrations of CO₃²⁻, *in situ* CO_{2(g)} and CO_{2(aq)} vary in the spacing where the local pH changes, and the distance of spacing is the most significant descriptor for the concentration of reactant, *in situ* CO_{2(g)}.

In a prior study,⁵ at a CEL:catalyst spacing of ~ 60 μm (Fig. 1f-g and Fig. S7), the volume fraction of CO_{2(g)} ([CO_{2(g)}]) at the plane of the catalyst was found to be ~ 2 vol.% with balanced gases of H₂ and C₂H₄ at current densities of 200-350 mA cm⁻² (Fig. 1c) – yet [CO_{2(g)}] is required to rise above 4 vol.% at the catalyst to reach a meaningful conversion rate of C₂₊ partial current densities of 100+ mA cm⁻² (Supplementary Note 3, 4 and Fig. S8).

We studied these effects further, noting that if the CEL and the catalyst are closely-spaced (Fig. 1d and e), the local pH at the CEL goes only as low as pH 10; CO₃²⁻ and OH⁻ diffusion neutralize the acidic CEL surface,^{29,30} leading to no *in situ* CO_{2(g)} generation at applied current densities of 200-350 mA cm⁻² (Fig. S9). In contrast, when we varied the CEL:catalyst spacing over the range 100-300 μm (Fig. 1h-k), we noted the opportunity to achieve the desired conditions of low pH (< 4) at the CEL for *in situ* CO_{2(g)} generation and [CO_{2(g)}] > 4 vol.% at the catalyst layer (CL) to trigger CO₂RR towards C₂₊ production. At the CL, the pH is above 13 since hydroxide ions are produced from CO₂RR. This high local pH accelerated the C-C coupling needed for C₂₊ to dominate over C₁.^{31,32} The pH gradient was measured using pH-sensitive dyes (Supplementary Note 5). We observed a progressive pH increase from pH ~2 at the CEL surface to ~12 at the edge of the interposer in the system designed for the experimental study of pH.

For the spacing range of 130-270 μm, optimal conditions, including [CO_{2(g)}] > 4 vol.% and the desired local pH, were achieved at the current density range 250-350 mA cm⁻², a regime of applied interest.^{33,34} In the case wherein the amount of carbonate is limited due to a small spacing, such as < 130 μm, there is no increase in the *in situ* CO_{2(g)} concentration at higher current densities (Fig. S3). However, the current density influences the rate of proton diffusion through the CEL: more protons diffuse at higher current densities and *in situ* CO_{2(g)} generally increases (Fig. 1c). Increasing the spacing to > 130 μm promotes carbonate-rich conditions, which provide more opportunities for protons to react with carbonate (Fig. S4-5). However, [CO_{2(g)}] decreases at a spacing > 540 μm due to an increased possibility of *in situ* CO₂ capture over long distances in the layer (Fig. S6).

Carbonate electrolysis system employing an interposer.



We then turned to the experimental implementation of these concepts (Fig. 1a). We needed an approach to construct a well-defined spacing – in effect, a stand-off – between the CEL and electrocatalyst. We used a hydrophilic membrane as an interposer and explored different interposer material compositions (Supplementary Note 6 and Fig. S10-12). We observed that C_{2+} FE was improved in a higher porosity system. We account for these observations via faster diffusion of species which enabled a higher concentration of $CO_{2(g)}$ at the CL.

In light of these findings, we focused on a hydrophilic mixed cellulose ester (MCE) interposer, a highly porous medium (material porosity > 84%) with a selection of thicknesses ranging from 130 μm to 540 μm (Fig. S13). We then moved to a cation exchange membrane (CEM) in the system to transport protons from the anodic oxygen evolution reaction (OER) (Fig. 2a) – an improvement that enabled reduced full cell potential compared to a BPM system (Fig. 2b). The CEM system may supply more protons to the cathodic side than the BPM system due to the concentration gradient, neutralizing the capture species (OH^-). However, we observed a similar product distribution for both the BPM system and CEM system (Fig. S14), indicating that excess proton diffusion in the CEM system is negligible when using 0.5 M H_2SO_4 as an analyte (Supplementary Note 7).

Experimentally, we first reconfirmed the findings of prior studies that, at $\sim 60 \mu\text{m}$ spacing, FE to C_{2+} resides below 14% at 250 mA cm^{-2} . When we optimized interposer thickness of 130-270 μm , we achieved a much-increased C_{2+} FE of 40% at 250 mA cm^{-2} (Fig. 2c). When the distance is smaller than 135 μm or larger than 540 μm , a lower rate of C_{2+} product generation is seen, the result of the limited concentration of *in situ* $CO_{2(g)}$ (Fig. 1c). In all cases, the only C_1 product detected was $HCOO^-$ with FE below 2%. No CO , CH_4 and CO_2 were detected for all applied current densities and different concentrations of carbonate electrolyte in the interposer system (Fig. 2d and Fig. S11). The product distribution, including high C_{2+} FE and negligible CO FE, was also observed in a simulated carbonate electrolysis system with CO_2 -depleted conditions (Supplementary Note 3). The experimental studies suggest that in the carbonate electrolysis system, low $[CO_{2(g)}]$ and slow *in situ* CO_2 flux contribute to steering C-C coupling by achieving locally concentrated CO and the enhanced residence time of CO . In the outlet stream, gaseous C_1 products and CO_2 were < 0.9 wt.% (0.1 vol.%) based on the detection limit of the gas chromatography: CO for 24 ppm, CH_4 for 56 ppm and CO_2 for 1000 ppm, respectively (Experimental procedures). To investigate whether carbonate was the source of carbon in electroreduction, we used ^{13}C labelled CO_3^{2-} , and the isotope experiment result ruled out any chemical reactions of interposer, cathode, and dissolved CO_2 (Fig. S15). To test for the possibility of chemical reactions related to the MCE membrane or its possible decomposition products, we compared electrochemical performance in two conditions: 1) carbonate electrolyte and 2) carbonate electrolyte with a dispersed MCE membrane in a PVDF interposer system (Fig. S16). In both cases, we observed a C_{2+} FE of $\sim 15\%$ at the applied current density of 200 and 300 mA cm^{-2} . We also conducted nuclear magnetic resonance (NMR) analysis to examine the chemical decomposition of the MCE membrane after long-term electrolysis of carbonate. We only detected signals for CO_2 -derived products, which supports that there is no chemical decomposition or reactions of MCE in the carbonate electrolysis system (Fig. S17)

Improved catalyst for carbonate electrolysis.

We turned to further system tuning towards increased C_{2+} FE. We posited that a portion of *in situ* CO_2 is converted into CO_3^{2-} at the catalyst surface due to the highly alkaline conditions.³¹ We, therefore, sought catalyst-design strategies to convert CO_2 to CO with faster kinetics at the catalyst surface to preserve the reactant. We used molecularly dispersed cobalt phthalocyanines on carbon nanotubes (CoPC-CNTs) known to produce CO from CO_2 with high turnover frequencies (Fig. 3a).^{35,36} We fabricated the layer-by-layer catalyst via airbrushing. The CoPC-CNTs layer is uniformly distributed on the Cu layer as shown in the scanning electron microscopy (SEM) image (Fig. 3b). X-ray photoelectron spectroscopy (XPS) and Energy-dispersive x-ray spectroscopy (EDS) confirm the existence of cobalt at the surface (Fig. S18-19).

The product distribution now showed a considerable further improvement: the C_{2+} total FE now rose to 47% at 300 mA cm^{-2} (Fig. 3c). The C_2H_4 FE is 34%, resulting in 56 wt.% of C_2H_4 in



the product gas stream due to the absence of gaseous C_1 products and unreacted CO_2 . The C_{2+} alcohols FE is 13% including 12% C_2H_5OH FE and 1% C_3H_7OH FE. As shown in Figure 3d, we achieve 140+ $mA\ cm^{-2}$ of C_{2+} partial current density at -4.1 V.

Continuous operation of capture-and-electrolysis system.

We then constructed a prototype that operates both CO_2 capture and electrolysis on a continuous basis (Fig. 4a and Fig. S20). The KOH capture liquid is regenerated during carbonate electrolysis as shown in the chemical balance (Fig. 2a and Supplementary Note 7). We recycled the resultant KOH solution to continuously capture additional CO_2 , converting it into K_2CO_3 . There are two reservoirs: the absorber is for CO_2 capture and the electrolyte reservoir provides the carbonate to the liquid-fed electrolyzer. Two reservoirs and the electrolyzer are connected by peripheral pumps circulating the capture liquid. During the electrolysis of carbonate into C_2H_4 and C_{2+} alcohols, generated OH^- returns to the absorber. We demonstrated capture-and-electrolysis sustained over 20 hours (Fig. 4b) at the current density of 200 $mA\ cm^{-2}$, with the C_{2+} FE consistently in the range of 36%-42%. The pH of reservoirs remains 11.8 for the absorber, 11.9 for the electrolyte and 1.8 for the anolyte (Table. S7). We found that, after 10 hours of operation, performance does show a decline (Fig. 4b). We studied the cause, finding that the pore structure of the MCE membrane degrades in alkali solution, producing an increase of full cell voltage and HER. It will be important to seek interposer materials that are stable under relevant conditions.

Economic assessments of carbonate electrolysis.

In Table 1, we offer an analysis that also estimates energy costs – associated with upstream generation for the gas-phase CO_2 and carbonate capture solutions, electrolysis, separation and carbonate regeneration – in systems including alkaline CO_2 electrolysis,³¹ neutral CO_2 electrolysis in a membrane electrode assembly (MEA),³⁷ acidic CO_2 electrolysis²³ vs. the present work (details in Supplementary Note 8). Both the gaseous CO_2 approaches in alkaline and neutral conditions experience a CO_2 utilization limit ($\leq 25\%$) since CO_2 gas is lost to carbonate formation, and carbonate crosses over to the anodic side during electrolysis.^{19,38} The product gas stream is diluted by unreacted CO_2 for all gas-phase CO_2 approaches. In comparison, the carbonate electrolysis system generates a product stream that does not contain CO_2 .

As is now well-established, alkaline electrolysis leads to a high rate of CO_2 loss – typically 95% is lost to carbonate and unreacted form – leading to an estimated 310 GJ/tonne of C_2H_4 for regeneration/separation energy costs. This cost is equal to 7 \times the lower heating value (LHV) of C_2H_4 .

Neutral CO_2RR still produces a high CO_2 stream in the cathodic outlet and this necessitates ~ 60 GJ/tonne of C_2H_4 investment in CO_2 separation from the cathode. Furthermore, CO_2 crossover mandates a separation of the O_2 -containing stream in the anodic outlet contributing to ~ 60 GJ/tonne of C_2H_4 of separation energy cost. The total separation cost is equal to 2 \times the LHV of C_2H_4 .

The acidic CO_2RR system enables an estimated decrease in product separation cost to ~ 18 GJ/tonne of C_2H_4 with a high CO_2 utilization efficiency of $\sim 76\%$. Unlike alkaline and neutral CO_2RR , no CO_2 is lost as carbonate formation and crossover, eliminating the need for processes to regenerate the carbonate or cross-overed CO_2 . However, there is a trade-off between FE and CO_2 utilization in presently-available acidic CO_2RR systems^{23,39}, with these systems still requiring energy-intensive DAC to generate gaseous CO_2 costing roughly ~ 28 GJ/tonne of C_2H_4 .

In contrast, the carbonate electrolysis to C_2H_4 system produces a CO_2 concentration that is undetectable in the cathode stream. This obviates the energy needed to separate CO_2 and C_2H_4 . What remains is 2 GJ/tonne of C_2H_4 to remove H_2 and H_2O from the cathodic outlet stream. The low separation cost originates from the high concentration of C_2H_4 and the absence of CO_2 . Furthermore, the system lowers the upstream generation cost by a factor of ~ 10 by bypassing the thermal swing of DAC.



We note the need to improve further the energy efficiency of the reactive capture electrolyzer itself. We offer that further studies of *in situ* CO₂ diffusion in the interposer, and further advances in interposer/electrocatalyst design, may contribute toward this goal.

DISCUSSION

Interposer and catalyst joint design enabled us herein to electroproduce 56 wt.% C₂H₄ from a carbonate solution with no detected CO₂ in the gas stream. To achieve this result, we focused on local pH and reactant concentration as metrics driving the performance of an electrochemical reactive capture system. The carbonate electrolysis system produces a gas stream that is undiluted by CO₂ and accomplishes complete CO₂ utilization, reducing regeneration/separation costs.

EXPERIMENTAL PROCEDURES

Resource Availability

Lead Contact

Further information and requests for resources should be directed to and will be fulfilled by the Lead Contact, Edward Sargent (ted.sargent@utoronto.ca).

Materials Availability

This study did not generate new unique reagents.

Data and Code Availability

The data presented in this work are available from the corresponding authors upon reasonable request.

Catalyst preparation

All reagents used in this work were purchased from suppliers without further purification. Cu catalysts (US Research Nanomaterials, Inc.) were prepared by spray-coating Cu nanoparticle ink onto carbon paper (Freudenberg H23, Fuel Cell Store). Cu nanoparticles (80 mg) were dispersed in a mixture of 12 mL methanol and 160 μ L Nafion solution and then sonicated for 3 hours. The Cu nanoparticle ink was spray-coated on the carbon paper with a loading of \sim 4 mg/cm² and dried under atmospheric conditions. The Cu catalysts were used for electrochemical characterization for carbonate electrolysis in a membrane electrode assembly (MEA) cell.

For simulated carbonate electrolysis experiments in a flow cell, Cu catalysts were prepared by spray-coating Cu nanoparticles onto a PTFE substrate (450 nm pore size). Cu nanoparticles (80 mg) were dispersed in a mixture of 12 mL methanol and 160 μ L Nafion solution and then sonicated for 3 hours. The Cu nanoparticle ink was spray-coated on the PTFE substrate with a loading of \sim 4 mg/cm² and dried under atmospheric conditions. CoPc, carboxylic acid-functionalized carbon nanotubes (CNTs) and Dimethylformamide (DMF) were purchased from Sigma Aldrich and used without further treatment. CoPc-CNTs catalyst was synthesized with modification from the previous report.³⁵ 30 mg of carboxylic acid-functionalized CNTs were dispersed in DMF (20 ml, solution 1) and sonicated for one hour. A calculated amount of CoPc was dispersed in DMF (20 ml, solution 2) and sonicated for one hour. Solutions 1 and 2 were mixed and sonicated for 30 min. After sonication, the mixture solution was stirred for 24 hours at room temperature. CoPc-CNTs were centrifuged and washed with DMF, ethanol and H₂O, followed by freeze-drying to obtain the final catalyst material.

CoPc-CNTs/Cu catalysts were prepared by spray-coating on the prepared Cu/carbon paper. CoPc-CNTs were dispersed in a mixture of 3 mL ethanol and 50 μ L Nafion solution and then sonicated for one hour. The CoPc-CNTs nanoparticle ink was spray-coated on the Cu/carbon paper with a loading of \sim 0.3 mg/cm² and dried under atmospheric conditions.

Electrochemical performance

Electrochemical data were collected using an electrochemical station (PGSTAT204) in an MEA system and a flow cell system. All experiments were repeated three times to enable reporting of the average and standard error. Electrolysis was maintained for at least 30 min prior to collecting gas and liquid samples. For the MEA system with carbonate electrolysis, the as-prepared Cu/carbon paper catalyst was used as the cathode in varying the distances between the cathode and a cation exchange membrane: 0, 135, 270 and 540 μ m with mixed



cellulose ester (MCE) membrane and varying catholyte: 0.5, 1, 1.5 and 2 M of K_2CO_3 . The anolyte was a 0.5 M H_2SO_4 solution. Titanium foam-supported iridium oxide (IrO_x/Ti) was used as the anode oxygen evolution reaction (OER) catalyst. Nafion 117 membrane was used to separate the two electrodes. The catholyte and anolyte were circulated using a peristaltic pump.

For the simulated carbonate electrolysis in a flow cell, the as-prepared Cu/PTFE catalyst was used as the working electrode in the catholyte (1.5 M of K_2CO_3) in varying gas-phase CO_2 partial pressure in the N_2 stream, maintaining the total flow rate of 50 sccm and gas-phase CO_2 flow rate. The anolyte was always a 1 M KOH solution. Ni foam and 3 M Ag/AgCl were used as the anode and reference electrodes, respectively. An anion exchange membrane (Fumasep FAA-3-PK-130) was used to separate the cathode and the anode. The catholyte and anolyte were circulated using a peristaltic pump.

The gas-phase products were analyzed using gas chromatography (GC) (Shimadzu 2014, PerkinElmer Clarus 580) equipped with a thermal conductivity detector (TCD) and a flame ionization detector (FID). All measurements were repeated three times to report the average and standard error. The liquid phase products were analyzed with a 600 MHz Agilent DD2 1H NMR.

The detection limit of GC for gas-phase products (CO and CH_4) is measured by varying the concentration of gas in the CO_2 stream. The ppm level of the gas-phase product is injected three times. The area of a peak is linearly correlated to the concentration when the area value is plotted at the y-axis, and the concentration is at the x-axis. The intercept of the x-axis represents of detection limits of gas concentration. The detection limit of CO_2 is measured by injecting a different air volume from 1 mL to 5 mL. The CO_2 concentration in the air is assumed at 400 ppm.

Material characterization

The Cu/CoPc-CNTs catalyst morphology was characterized by field emission scanning electron microscopy (Hitachi, SU5000). The surface composition was analyzed with ThermoFisher Scientific K-alpha X-ray photoelectron spectroscopy using Al K α X-ray radiation. XPS spectra were calibrated with the C 1s peak at 284.5 eV. SEM-EDS was conducted by JEOL JSM-7900FLV SEM at an accelerating voltage of 10 kV with backscattered electron detection, which is equipped with a light-element X-ray detector and an Oxford Aztec energy-dispersive X-ray analysis system.

Fluorescence measurements

For the simulated interposer system in a H-cell, a carbon paper, Pt mesh, and Ag/AgCl reference electrode were used as the working, counter, and reference electrodes, respectively. 0.2 M K_2CO_3 and 0.5 M H_2SO_4 electrolytes were used as a catholyte and an anolyte, respectively. Nafion 117 membrane was used to separate the cathode part and the anode part. Molecular Probes LysoSensor Green DND 189 (LSG) was used to measure a pH range of 1-6, and 5(6)-Carboxynaphthofluorescein (CNF) was used to measure neutral and alkaline pH from 6 to 14. Using 365 nm of UV light, the fluorescence emissions were collected with a spectrometer (Ocean Optics, QE Pro)

Stability test

Two reservoirs were connected by peristaltic pumps (Fig. S17). CO_2 is purged into the absorber with 3 M KOH until the pH of the solution reaches to ~ 12 , and an electrolyte reservoir provides the carbonate solution to the electrolyzer. The carbonate electrolyte is pumped to the MEA cell with no gas purging. The regenerated KOH solution returns to the absorber, where it captures CO_2 in the form of CO_3^{2-} . The gas products from the electrolyte reservoir were monitored with gas chromatography injection.

ACKNOWLEDGMENTS

This work was financially supported by the Ontario Research Foundation: Research Excellence Program, the Natural Sciences and Engineering Research Council (NSERC) of Canada

AUTHOR CONTRIBUTIONS

E.H.S. supervised the work. G.L. contributed to the main idea and designed experiments. A.S.R. contributed to multiphysic modeling. B.H.L. fabricated the electrocatalyst and contributed to material characterization. J.Z, D.H.W. and Y.C.X. contributed to the electrochemical experiments. J.P.E. and Y.Z performed the energy analysis. M.G.L. conducted C13 labelling



experiments. E.D.J conducted local pH measurements. J.A., S.P. and H.L conducted material characterization. F.A. performed voltage breakdown analysis. T.A. and S.L. assisted in the multiphysic modeling. I.G., R.K.M, R.D., C.P.O., Z.C. and D.S. contributed to data analysis and manuscript preparation. H.L. and E.H.S acknowledge the financial support from Northwestern University start-up grant.

DECLARATION OF INTERESTS

The authors declare no competing interests.

REFERENCES

- Brethomé, F.M., Williams, N.J., Seipp, C.A., Kidder, M.K., and Custelcean, R. (2018). Direct air capture of CO₂ via aqueous-phase absorption and crystalline-phase release using concentrated solar power. *Nature Energy* 3, 553-559. 10.1038/s41560-018-0150-z.
- Kätelhön, A., Meys, R., Deutz, S., Suh, S., and Bardow, A. (2019). Climate change mitigation potential of carbon capture and utilization in the chemical industry. *Proceedings of the National Academy of Sciences* 116, 11187-11194. doi:10.1073/pnas.1821029116.
- Socolow, R., Desmond, M., Aines, R., Blackstock, J., Bolland, O., Kaarsberg, T., Lewis, N., Mazzotti, M., Pfeiffer, A., and Sawyer, K. (2011). Direct air capture of CO₂ with chemicals: a technology assessment for the APS Panel on Public Affairs. American Physical Society.
- Lee, G., Li, Y.C., Kim, J.-Y., Peng, T., Nam, D.-H., Sedighian Rasouli, A., Li, F., Luo, M., Ip, A.H., Joo, Y.-C., and Sargent, E.H. (2021). Electrochemical upgrade of CO₂ from amine capture solution. *Nature Energy* 6, 46-53. 10.1038/s41560-020-00735-z.
- Li, Y.C., Lee, G., Yuan, T., Wang, Y., Nam, D.-H., Wang, Z., Garcia de Arquer, F.P., Lum, Y., Dinh, C.-T., Voznyy, O., and Sargent, E.H. (2019). CO₂ Electroreduction from Carbonate Electrolyte. *ACS Energy Letters* 4, 1427-1431. 10.1021/acenergylett.9b00975.
- Li, T., Lees, E.W., Goldman, M., Salvatore, D.A., Weekes, D.M., and Berlinguette, C.P. (2019). Electrolytic Conversion of Bicarbonate into CO in a Flow Cell. *Joule* 3, 1487-1497. <https://doi.org/10.1016/j.joule.2019.05.021>.
- Zhang, Z., Lees, E.W., Habibzadeh, F., Salvatore, D.A., Ren, S., Simpson, G.L., Wheeler, D.G., Liu, A., and Berlinguette, C.P. (2022). Porous metal electrodes enable efficient electrolysis of carbon capture solutions. *Energy & Environmental Science* 15, 705-713. 10.1039/D1EE02608A.
- Xiao, Y.C., Gabardo, C.M., Liu, S., Lee, G., Zhao, Y., O'Brien, C.P., Miao, R.K., Xu, Y., Edwards, J.P., and Fan, M. (2023). Direct carbonate electrolysis into pure syngas. *EES Catalysis*.
- Kar, S., Goepfert, A., and Prakash, G.K.S. (2019). Integrated CO₂ Capture and Conversion to Formate and Methanol: Connecting Two Threads. *Accounts of Chemical Research* 52, 2892-2903. 10.1021/acs.accounts.9b00324.
- Kothandaraman, J., Saavedra Lopez, J., Jiang, Y., Walter, E.D., Burton, S.D., Dagle, R.A., and Heldebrant, D.J. (2021). Integrated Capture and Conversion of CO₂ to Methane Using a Water-lean, Post-Combustion CO₂ Capture Solvent. *ChemSusChem* 14, 4812-4819. <https://doi.org/10.1002/cssc.202101590>.
- Sen, R., Goepfert, A., Kar, S., and Prakash, G.K.S. (2020). Hydroxide Based Integrated CO₂ Capture from Air and Conversion to Methanol. *Journal of the American Chemical Society* 142, 4544-4549. 10.1021/jacs.9b12711.
- The global ethanol market size is expected to be worth around USD 155.6 billion by 2030 from USD 93.7 billion in 2020, growing at a CAGR of 5.2% from 2021 to 2030. Increasing usage of ethyl alcohol as biofuel is major factor driving growth of the ethanol market. (2021). <https://www.globenewswire.com/news-release/2021/01/18/2160198/0/en/Ethanol-Market-Size-Worth-Around-USD-155-6-Billion-by-2030.html#:~:text=The%20global%20ethanol%20market%20size,5.2%20%20from%202021%20to%202030> Q PrecedenceResearch.
- Ethylene Market Size Worth \$230.7 Billion By 2029 | CAGR: 5.5%. (2021). <https://www.polarismarketresearch.com/press-releases/ethylene-market> Polaris.
- Feed Acidifiers Market Size Worth \$2.03 Billion By 2026 | CAGR: 4.5%. (2017). <https://www.polarismarketresearch.com/press-releases/feed-acidifiers-market> Polaris.
- Carbon Dioxide Market Size Worth \$9.91 Billion by 2029 | CAGR: 4.1%. (2021). <https://www.polarismarketresearch.com/press-releases/carbon-dioxide-co2-market> Polaris.
- Keith, D.W., Holmes, G., St. Angelo, D., and Heidel, K. (2018). A Process for Capturing CO₂ from the Atmosphere. *Joule* 2, 1573-1594. <https://doi.org/10.1016/j.joule.2018.05.006>.
- Arquer, F.P.G.d., Dinh, C.-T., Ozden, A., Wicks, J., McCallum, C., Kirmani, A.R., Nam, D.-H., Gabardo, C., Seifitokaldani, A., Wang, X., et al. (2020). CO₂ electrolysis to multicarbon products at activities greater than 1 A cm⁻². *Science* 367, 661-666. doi:10.1126/science.aay4217.
- Li, F., Thevenon, A., Rosas-Hernández, A., Wang, Z., Li, Y., Gabardo, C.M., Ozden, A., Dinh, C.T., Li, J., Wang, Y., et al. (2020). Molecular tuning of CO₂-to-ethylene conversion. *Nature* 577, 509-513. 10.1038/s41586-019-1782-2.
- Rabinowitz, J.A., and Kanan, M.W. (2020). The future of low-temperature carbon dioxide electrolysis depends on solving one basic problem. *Nature Communications* 11, 1-3.
- Alerte, T., Edwards, J.P., Gabardo, C.M., O'Brien, C.P., Gaona, A., Wicks, J., Obradović, A., Sarkar, A., Jaffer, S.A., MacLean, H.L., et al. (2021). Downstream of the CO₂ Electrolyzer: Assessing the Energy Intensity of Product Separation. *ACS Energy Letters* 6, 4405-4412. 10.1021/acenergylett.1c02263.
- Huang, J.E., Li, F., Ozden, A., Rasouli, A.S., Arquer, F.P.G.d., Liu, S., Zhang, S., Luo, M., Wang, X., Lum, Y., et al. (2021). CO₂ electrolysis to multicarbon products in strong acid. *Science* 372, 1074-1078. doi:10.1126/science.abg6582.
- O'Brien, C.P., Miao, R.K., Liu, S., Xu, Y., Lee, G., Robb, A., Huang, J.E., Xie, K., Bertens, K., Gabardo, C.M., et al. (2021). Single Pass CO₂ Conversion Exceeding 85% in the Electrosynthesis of Multicarbon Products via Local CO₂ Regeneration. *ACS Energy Lett.* 6, 2952-2959. 10.1021/acenergylett.1c01122.
- Zhao, Y., Hao, L., Ozden, A., Liu, S., Miao, R.K., Ou, P., Alkayyali, T., Zhang, S., Ning, J., Liang, Y., et al. (2023). Conversion of CO₂ to multicarbon products in strong acid by controlling the catalyst microenvironment. *Nature Synthesis*. 10.1038/s44160-022-00234-x.
- Gabardo, C.M., O'Brien, C.P., Edwards, J.P., McCallum, C., Xu, Y., Dinh, C.-T., Li, J., Sargent, E.H., and Sinton, D. (2019). Continuous Carbon Dioxide Electroreduction to Concentrated Multi-carbon Products Using a Membrane Electrode Assembly. *Joule* 3, 2777-2791. <https://doi.org/10.1016/j.joule.2019.07.021>.
- Kim, C., Bui, J.C., Luo, X., Cooper, J.K., Kusoglu, A., Weber, A.Z., and Bell, A.T. (2021). Tailored catalyst microenvironments for CO₂ electroreduction to multicarbon products on copper using bilayer ionomer coatings. *Nature Energy* 6,

- 1026-1034. 10.1038/s41560-021-00920-8.
26. Idem, R., Supap, T., Shi, H., Gelowitz, D., Ball, M., Campbell, C., and Tontiwachwuthikul, P. (2015). Practical experience in post-combustion CO₂ capture using reactive solvents in large pilot and demonstration plants. *International Journal of Greenhouse Gas Control* 40, 6-25. <https://doi.org/10.1016/j.ijggc.2015.06.005>.
27. Lin, Y.-J., and Rochelle, G.T. (2016). Approaching a reversible stripping process for CO₂ capture. *Chemical Engineering Journal* 283, 1033-1043. <https://doi.org/10.1016/j.cej.2015.08.086>.
28. Greenblatt, J.B., Miller, D.J., Ager, J.W., Houle, F.A., and Sharp, I.D. (2018). The Technical and Energetic Challenges of Separating (Photo)Electrochemical Carbon Dioxide Reduction Products. *Joule* 2, 381-420. <https://doi.org/10.1016/j.joule.2018.01.014>.
29. Lees, E.W., Bui, J.C., Song, D., Weber, A.Z., and Berlinguette, C.P. (2022). Continuum Model to Define the Chemistry and Mass Transfer in a Bicarbonate Electrolyzer. *ACS Energy Letters* 7, 834-842. 10.1021/acsenergylett.1c02522.
30. Kas, R., Yang, K., Yewale, G.P., Crow, A., Burdyny, T., and Smith, W.A. (2022). Modeling the Local Environment within Porous Electrode during Electrochemical Reduction of Bicarbonate. *Industrial & Engineering Chemistry Research*. 10.1021/acs.iecr.2c00352.
31. Dinh, C.-T., Burdyny, T., Kibria, M.G., Seifitokaldani, A., Gabardo, C.M., Arquer, F.P.G.d., Kiani, A., Edwards, J.P., Luna, P.D., Bushuyev, O.S., et al. (2018). CO₂ electroreduction to ethylene via hydroxide-mediated copper catalysis at an abrupt interface. *Science* 360, 783-787. doi:10.1126/science.aas9100.
32. Varela, A.S., Kroschel, M., Reier, T., and Strasser, P. (2016). Controlling the selectivity of CO₂ electroreduction on copper: The effect of the electrolyte concentration and the importance of the local pH. *Catalysis Today* 260, 8-13. <https://doi.org/10.1016/j.cattod.2015.06.009>.
33. Jouny, M., Luc, W., and Jiao, F. (2018). General Techno-Economic Analysis of CO₂ Electrolysis Systems. *Industrial & Engineering Chemistry Research* 57, 2165-2177. 10.1021/acs.iecr.7b03514.
34. Shin, H., Hansen, K.U., and Jiao, F. (2021). Techno-economic assessment of low-temperature carbon dioxide electrolysis. *Nature Sustainability* 4, 911-919. 10.1038/s41893-021-00739-x.
35. Zhang, X., Wang, Y., Gu, M., Wang, M., Zhang, Z., Pan, W., Jiang, Z., Zheng, H., Lucero, M., Wang, H., et al. (2020). Molecular engineering of dispersed nickel phthalocyanines on carbon nanotubes for selective CO₂ reduction. *Nature Energy* 5, 684-692. 10.1038/s41560-020-0667-9.
36. Li, F., Li, Y.C., Wang, Z., Li, J., Nam, D.-H., Lum, Y., Luo, M., Wang, X., Ozden, A., Hung, S.-F., et al. (2020). Cooperative CO₂-to-ethanol conversion via enriched intermediates at molecule-metal catalyst interfaces. *Nature Catalysis* 3, 75-82. 10.1038/s41929-019-0383-7.
37. Ozden, A., Li, F., Garcia de Arquer, F.P., Rosas-Hernández, A., Thevenon, A., Wang, Y., Hung, S.-F., Wang, X., Chen, B., Li, J., et al. (2020). High-Rate and Efficient Ethylene Electrosynthesis Using a Catalyst/Promoter/Transport Layer. *ACS Energy Letters* 5, 2811-2818. 10.1021/acsenergylett.0c01266.
38. Mardle, P., Cassegrain, S., Habibzadeh, F., Shi, Z., and Holdcroft, S. (2021). Carbonate Ion Crossover in Zero-Gap, KOH Anolyte CO₂ Electrolysis. *The Journal of Physical Chemistry C* 125, 25446-25454. 10.1021/acs.jpcc.1c08430.
39. Huang, J.E., Li, F., Ozden, A., Sedighian Rasouli, A., Garcia de Arquer, F.P., Liu, S., Zhang, S., Luo, M., Wang, X., and Lum, Y. (2021). CO₂ electrolysis to multicarbon products in strong acid. *Science* 372, 1074-1078.

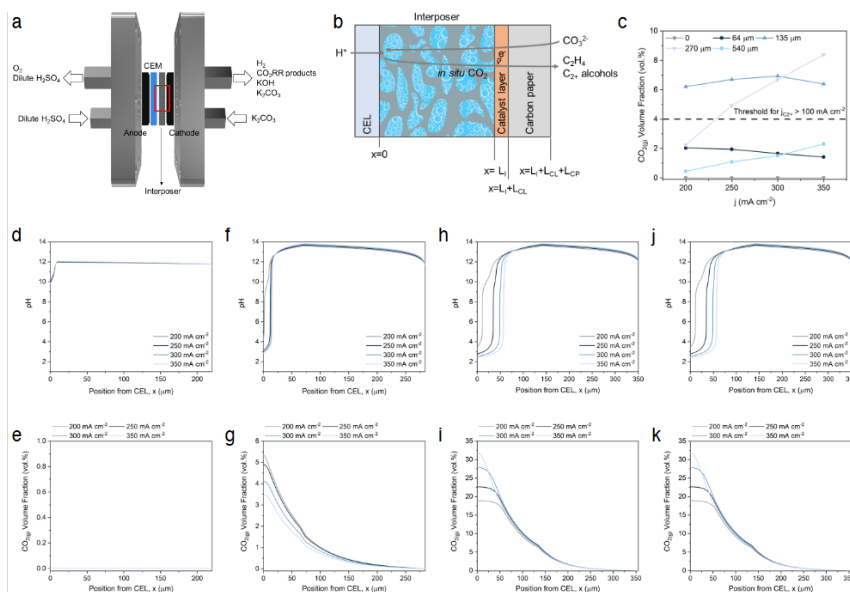
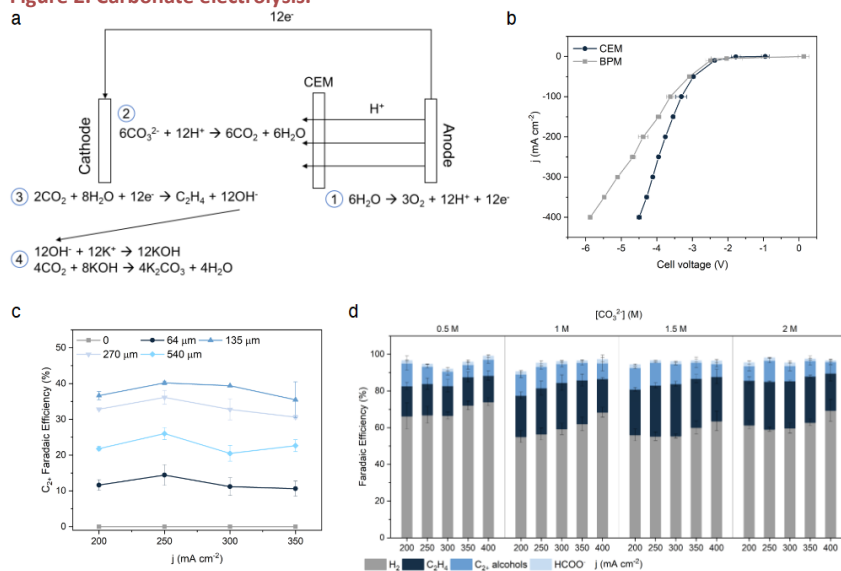


Figure 1. Carbonate electrolysis system employing an interposer.

(a) System diagram of CO₃²⁻-fed electrolyzer. The cathode and anode are separated by the cation exchange membrane (CEM) and the mixed cellulose ester (MCE) membrane as the interposer. K₂CO₃ is fed to the electrolyzer and *in situ* CO₂ is converted into CO₂-derived products. KOH is generated at the cathode from *in situ* CO₂ reduction reaction (CO₂RR). 0.5 M H₂SO₄ is fed at the anode, and the anodic oxygen evolution reaction supplies protons. (b) Schematic of cation exchange layer (CEL), the interposer, catalyst layer (CL) and carbon paper (CP). The MCE membrane has a pore where the carbonate liquid phase and gas-phase *in situ* CO₂ are distributed. (c) CO_{2(g)} volume fraction for different spacing (L_i) conditions, 0, 64, 135, and 540 μm at current densities of 200, 250, 300, and 350 mA cm⁻² in 1.5 M of K₂CO₃ electrolyte. (d, f, h, j) pH profile of 0, 64, 135, and 540 μm spacing respectively at the applied current densities from 200 mA cm⁻² to 350 mA cm⁻² in 1.5 M of K₂CO₃ electrolyte. (e, g, i, k) *in situ* CO_{2(g)} volume fraction profile of 0, 64, 135, and 540 μm spacing respectively at the applied current densities from 200 mA cm⁻² to 350 mA cm⁻² in 1.5 M K₂CO₃ electrolyte.

Figure 2. Carbonate electrolysis.



(a) Chemical reactions of carbonate electrolysis with the cation exchange membrane (CEM). OER at the anodic side supplies protons to the cathodic side. Carbonate is converted into *in situ* CO₂ via the carbonate/proton reactions. CO₂ reduction reaction (CO₂RR) occurs with a Cu electrocatalyst. CO₂-derived products are generated and OH⁻ is produced during *in situ* CO₂RR. Unreacted CO₂ is captured by OH⁻. (b) Full cell j-V curve with Cu electrocatalyst with a CEM and a bipolar membrane (BPM) in 1.5 M of K₂CO₃ electrolyte with 135 μm interposer. Higher voltage is observed in the case of the BPM system compared to the CEM system due to water dissociation overpotential. (c) C₂₊ Faradaic efficiency (FE) of carbonate electrolysis with Cu electrocatalyst in 1.5 M of K₂CO₃ electrolyte with the different thickness of interposer from 0 to 540 μm. (d) Product distribution for different concentrations of K₂CO₃ electrolyte from 0.5 M to 2 M with a 135 μm interposer. C₂₊ alcohols Faradaic efficiency includes C₂H₅OH and C₃H₇OH.

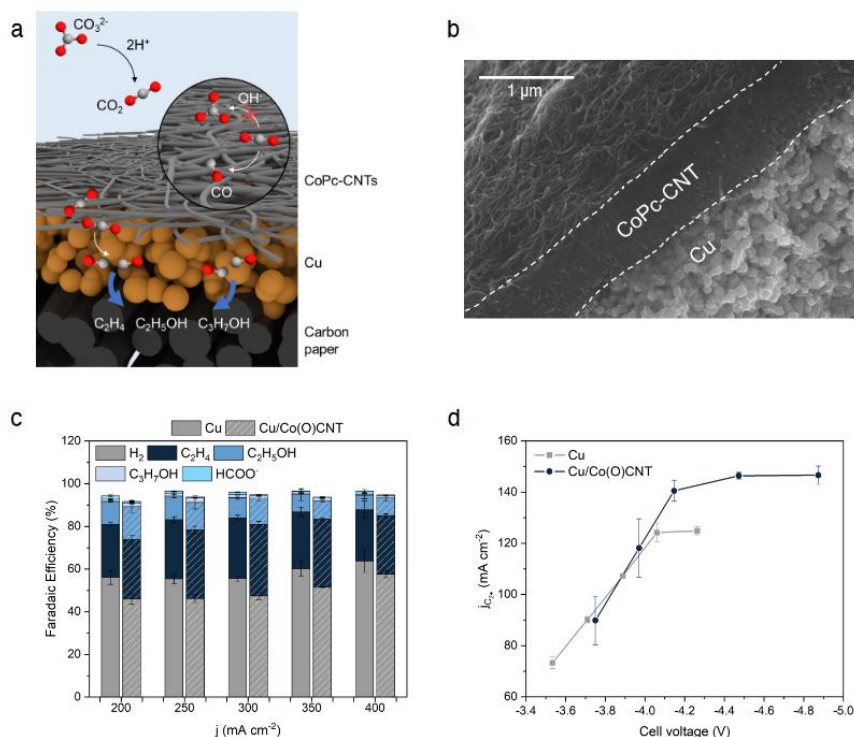


Figure 3. Electrochemical performance of improved catalyst for carbonate electrolysis.

(a) Illustration of the improved catalyst depositing CoPc-CNTs layer onto Cu electrocatalyst.

(b) Scanning electron microscope image of Cu/CoPc-CNTs layer.

(c) Product distribution of control Cu electrocatalyst and Cu/CoPC-CNTs catalyst at applied current densities from 200 mA cm^{-2} to 400 mA cm^{-2} . 1.5 M K_2CO_3 and 135 μm MCE membrane are used as the electrolyte and interposer, respectively.

(d) C_2^+ partial current density versus full cell voltage for Cu electrocatalyst and Cu/CoPc-CNTs electrocatalyst.

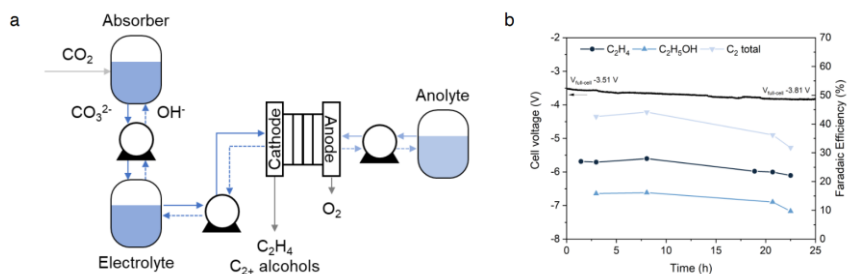


Figure 4. Extended operation with CO₂ capture liquid stream.

(a) The schematic illustrates the process flow of the capture-and-electrolysis system. CO₂ is captured with 3 M KOH at the absorber until the pH of the solution reaches to ~12, and the capture liquid, K₂CO₃, is fed to the electrolyzer. The lean capture liquid, KOH, returns to the absorber. (b) Long-term operation for the capture-and-electrolysis system. The experiment was performed with a Cu/CoPc-CNTs electrocatalyst and 135 μm interposer. Cell voltage and Faradaic efficiency of C₂H₄, C₂H₅OH, and C₂₊ products are noted during the operation.

Table 1. Title without Reference or Footnote Citations

System	Alkaline CO ₂ RR	Neutral CO ₂ RR	Acidic CO ₂ RR	Carbonate electrolysis
Full cell voltage (V)	2.4	3.9	3.4	4.1
C ₂ H ₄ selectivity (%)	70	66	24	34
Current density (mA cm ⁻²)	150	315	200	300
Energy efficiency (%)	34	19	8	10
CO ₂ utilization (%)	5	11	76	100 ^a
C ₂ H ₄ concentration at the outlet (wt.%)	4	8	19	56
CO ₂ concentration at the outlet (wt.%)	93	88	56	0
Energy cost (GJ/tonne of C ₂ H ₄)				
Upstream generation	28	28	28	3
Electrolysis	142	244	586	499
Product separation	115	55	18	2
Anode separation	0	57	0	0
Carbonate generation	198	0	0	0
Total	483	384	631	504

Energy analysis of separation and carbonate regeneration cost in different systems, alkaline CO₂RR in a flow cell, neutral CO₂RR in a membrane electrode assembly (MEA) cell acidic CO₂RR in a flow cell and carbonate electrolysis.

^aNo detectable CO₂ gas in the cathodic/anodic tail gas.

SUPPLEMENTAL INFORMATION

Document S1. Supplemental Note 1–9, Figures S1–S32, and Table S1–7